



# Elastic differential cross-section $d\sigma/dt$ at $\sqrt{s} = 2.76$ TeV and implications on the existence of a colourless C-odd three-gluon compound state

G. Antchev<sup>20</sup>, P. Aspell<sup>17</sup>, I. Atanassov<sup>20</sup>, V. Avati<sup>15</sup>, J. Baechler<sup>17</sup>, C. Baldenegro Barrera<sup>19</sup>, V. Berardi<sup>8,9</sup>, M. Berretti<sup>4</sup>, E. Bossini<sup>14</sup>, U. Bottigli<sup>14</sup>, M. Bozzo<sup>11,12</sup>, H. Burkhardt<sup>17</sup>, F. S. Cafagna<sup>8</sup>, M. G. Catanesi<sup>8</sup>, M. Csanád<sup>6,21</sup>, T. Csörgő<sup>6,7</sup>, M. Deile<sup>17</sup>, F. De Leonardis<sup>8,10</sup>, M. Doubek<sup>3</sup>, D. Druzhkin<sup>17</sup>, K. Eggert<sup>18</sup>, V. Eremin<sup>22</sup>, F. Ferro<sup>11</sup>, A. Fiergolski<sup>17</sup>, F. Garcia<sup>4</sup>, V. Georgiev<sup>1</sup>, S. Giani<sup>17</sup>, L. Grzanka<sup>15</sup>, J. Hammerbauer<sup>1</sup>, V. Ivanchenko<sup>16</sup>, J. Kašpar<sup>2,13</sup>, J. Kopal<sup>17</sup>, V. Kundrať<sup>2</sup>, S. Lami<sup>13</sup>, G. Latino<sup>14</sup>, R. Lauhakangas<sup>4</sup>, C. Lindsey<sup>19</sup>, M. V. Lokajčiček<sup>2</sup>, L. Losurdo<sup>14</sup>, M. Lo Vetere<sup>11,12</sup>, F. Lucas Rodríguez<sup>17</sup>, M. Macrí<sup>11</sup>, M. Malawski<sup>15</sup>, N. Minafra<sup>19</sup>, S. Minutoli<sup>11</sup>, T. Naaranoja<sup>4,5</sup>, F. Nemes<sup>6,17,a</sup>, H. Niewiadomski<sup>18</sup>, T. Novák<sup>7</sup>, E. Oliveri<sup>17</sup>, F. Oljemark<sup>4,5</sup>, M. Oriunno<sup>23</sup>, K. Österberg<sup>4,5</sup>, P. Palazzi<sup>17</sup>, V. Passaro<sup>8,10</sup>, Z. Peroutka<sup>1</sup>, J. Procházka<sup>3</sup>, M. Quinto<sup>8,9</sup>, E. Radermacher<sup>17</sup>, E. Radicioni<sup>8</sup>, F. Ravotti<sup>17</sup>, E. Robutti<sup>11</sup>, C. Royon<sup>19</sup>, G. Ruggiero<sup>17</sup>, H. Saarikko<sup>4,5</sup>, A. Scribano<sup>13</sup>, J. Smajek<sup>17</sup>, W. Snoeys<sup>17</sup>, J. Sziklai<sup>6</sup>, C. Taylor<sup>18</sup>, E. Tcherniaev<sup>16</sup>, N. Turini<sup>14</sup>, V. Vacek<sup>3</sup>, J. Welti<sup>4,5</sup>, J. Williams<sup>19</sup>

- <sup>1</sup> University of West Bohemia, Pilsen, Czech Republic  
<sup>2</sup> Institute of Physics of the Academy of Sciences of the Czech Republic, Prague, Czech Republic  
<sup>3</sup> Czech Technical University, Prague, Czech Republic  
<sup>4</sup> Helsinki Institute of Physics, University of Helsinki, Helsinki, Finland  
<sup>5</sup> Department of Physics, University of Helsinki, Helsinki, Finland  
<sup>6</sup> Wigner Research Centre for Physics, RMKI, Budapest, Hungary  
<sup>7</sup> EKV KRC, Gyöngyös, Hungary  
<sup>8</sup> INFN Sezione di Bari, Bari, Italy  
<sup>9</sup> Dipartimento Interateneo di Fisica di Bari, Bari, Italy  
<sup>10</sup> Dipartimento di Ingegneria Elettrica e dell'Informazione-Politecnico di Bari, Bari, Italy  
<sup>11</sup> INFN Sezione di Genova, Genoa, Italy  
<sup>12</sup> Università degli Studi di Genova, Genoa, Italy  
<sup>13</sup> INFN Sezione di Pisa, Pisa, Italy  
<sup>14</sup> Università degli Studi di Siena and Gruppo Collegato INFN di Siena, Siena, Italy  
<sup>15</sup> AGH University of Science and Technology, Kraków, Poland  
<sup>16</sup> Tomsk State University, Tomsk, Russia  
<sup>17</sup> CERN, Geneva, Switzerland  
<sup>18</sup> Department of Physics, Case Western Reserve University, Cleveland, OH, USA  
<sup>19</sup> The University of Kansas, Lawrence, USA  
<sup>20</sup> INRNE-BAS, Institute for Nuclear Research and Nuclear Energy, Bulgarian Academy of Sciences, Sofia, Bulgaria  
<sup>21</sup> Department of Atomic Physics, ELTE University, Budapest, Hungary  
<sup>22</sup> Ioffe Physical-Technical Institute of Russian Academy of Sciences, St. Petersburg, Russian Federation  
<sup>23</sup> SLAC National Accelerator Laboratory, Stanford, CA, USA

Received: 20 August 2019 / Accepted: 15 January 2020 / Published online: 5 February 2020  
© The Author(s) 2020

**Abstract** The proton–proton elastic differential cross section  $d\sigma/dt$  has been measured by the TOTEM experiment at  $\sqrt{s} = 2.76$  TeV energy with  $\beta^* = 11$  m beam optics. The Roman Pots were inserted to 13 times the transverse beam size from the beam, which allowed to measure the differential cross-section of elastic scattering in a range of the squared

four-momentum transfer ( $|t|$ ) from 0.36 to 0.74 GeV<sup>2</sup>. The differential cross-section can be described with an exponential in the  $|t|$ -range between 0.36 and 0.54 GeV<sup>2</sup>, followed by a diffractive minimum (dip) at  $|t_{\text{dip}}| = (0.61 \pm 0.03)$  GeV<sup>2</sup> and a subsequent maximum (bump). The ratio of the  $d\sigma/dt$  at the bump and at the dip is  $1.7 \pm 0.2$ . When compared to the proton–antiproton measurement of the D0 experiment at  $\sqrt{s} = 1.96$  TeV, a significant difference can be observed. Under the condition that the effects due to the energy differ-

M. L. Vetere: Deceased.

<sup>a</sup>e-mail: fnemes@cern.ch

ence between TOTEM and D0 can be neglected, the result provides evidence for the exchange of a colourless C-odd three-gluon compound state in the  $t$ -channel of the proton–proton and proton–antiproton elastic scattering.

## 1 Introduction

This article presents the first measurement of the proton–proton (pp) elastic differential cross section  $d\sigma/dt$  at a centre-of-mass energy  $\sqrt{s} = 2.76$  TeV. The four-momentum transfer squared ( $|t|$ ) range of the measured differential cross-section  $d\sigma/dt$  includes the diffractive minimum. The TOTEM collaboration has previously measured proton–proton elastic scattering at energies 7 TeV, 8 TeV and 13 TeV [1–9]. The importance of the present article is that it constitutes the pp  $d\sigma/dt$  measurement closest to a corresponding proton–antiproton ( $p\bar{p}$ ) measurement at the TeV scale, since the D0 measurement at Fermilab is at a comparable energy  $\sqrt{s} = 1.96$  TeV [10]. The predominant Pomeron contribution to elastic pp scattering is crossing even. Any difference between the pp and  $p\bar{p}$  differential cross-section at the TeV scale may be an evidence for a crossing-odd exchange, the Odderon, introduced in [11, 12] and predicted in QCD as the exchange of a colourless C-odd three-gluon compound state [13–17], for reviews see [18, 19]. At the TeV energy scale, any possible other contribution by Reggeons is expected to be below the percent level [20]. For completeness, an exchange of a 3-gluon state may also be crossing even, e.g. in case the state evolves (collapses) into 2 gluons [17, 19]. However hereafter, unless specified differently, we will refer only to crossing-odd 3-gluon exchanges – the crossing-even 3-gluon exchanges will be included in the Pomeron amplitude as a sub-leading contribution (suppressed by  $\alpha_s$  with respect to the 2-gluon exchanges).

Section 2 outlines the experimental apparatus used for this measurement. Section 3 summarises the data-taking conditions including details of the kinematics reconstruction, alignment and beam optics. The differential cross-section is described in Sect. 4 followed by a discussion of the physics results in Sect. 5.

## 2 Experimental apparatus

The TOTEM experimental setup consists of two inelastic telescopes T1 and T2 to detect charged particles coming from inelastic pp collisions and the Roman Pot detectors (RP) to detect elastically scattered protons at very small angles. The inelastic telescopes are placed symmetrically on both sides of Interaction Point 5 (IP5): the T1 telescope is based on cathode strip chambers (CSCs) placed at  $\pm 9$  m and covers the pseudorapidity range  $3.1 \leq |\eta| \leq 4.7$ ; the T2

telescope is based on gas electron multiplier (GEM) chambers placed at  $\pm 13.5$  m and covers the pseudorapidity range  $5.3 \leq |\eta| \leq 6.5$ . The pseudorapidity coverage of the two telescopes at  $\sqrt{s} = 2.76$  TeV allows the detection of about 96 % of the inelastic events. As the fraction of events with all final state particles beyond the instrumented region has to be estimated using phenomenological models, the excellent acceptance in TOTEM minimizes the dependence on such models and thus provides small uncertainty on the inelastic rate measurement.

The Roman Pot (RP) units used for the present measurement are located on both sides of the IP at distances of  $\pm 214.6$  m (near) and  $\pm 220.0$  m (far) from IP5, see Fig. 1. A unit consists of 3 RPs, two approaching the outgoing beam vertically and one horizontally. The horizontal RP detectors were not inserted during this particular data taking and the vertical alignment uses the RP position sensors and is further refined with precise constraints based on symmetries of elastic scattering [21]. The 5.4 m long lever arm between the near and the far RP units has the important advantage that the local track angles in the  $x$  and  $y$ -projections perpendicular to the beam direction can be reconstructed with a precision of  $2 \mu\text{rad}$ . A complete description of the TOTEM detector system is given in [22, 23].

Each RP is equipped with a stack of 10 silicon strip detectors designed with the specific objective of reducing the insensitive area at the edge facing the beam to only a few tens of micrometres. The 512 strips with  $66 \mu\text{m}$  pitch of each detector are oriented at an angle of  $+45^\circ$  (five planes) and  $-45^\circ$  (five planes) with respect to the detector edge facing the beam [24].

## 3 Data taking and analysis

The analysis is performed on a data sample (DS1) recorded in 2013 during an LHC fill with  $\beta^* = 11$  m injection optics [25–27]. The RP detectors were inserted to 13 times the transverse beam size. Although in this work we focus on the analysis of DS1, the present analysis uses the total cross-section measurement at  $\sqrt{s} = 2.76$  TeV (data set DS2) recorded with RP detectors placed at 4.3 times the transverse beam size, in order to obtain its final normalization [7, 21, 28]. The differential cross-section of DS2 covers the  $|t|$  range from 0.07 to  $0.475 \text{ GeV}^2$  and it is included in this article for the sake of completeness, see Table 3, although its detailed description is provided elsewhere [21, 28].

The vertical RP detectors were at 13 times the transverse beam size ( $\sigma_{\text{beam}}$ ) from the outgoing beams. The collected events have been triggered by the T2 telescope in either arm (inelastic trigger), by the RP detectors in a double-arm coincidence (elastic trigger), and by random bunch crossings (zero-bias sample used for calibration).

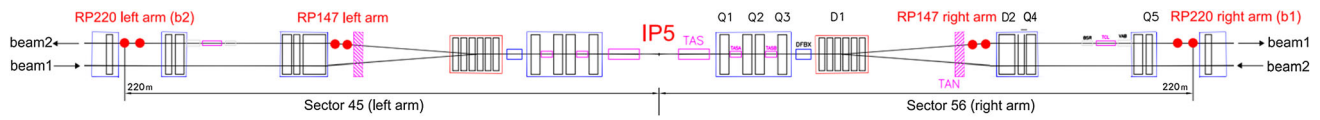


**Fig. 1** Schematic layout of the LHC from IP5 up to the “near” and “far” Roman Pot units, where the near and far pots are indicated by full (red) dots on beams 1 and 2

### 3.1 Elastic analysis

#### 3.1.1 Reconstruction of kinematics

The horizontal and vertical scattering angles of the proton at IP5 ( $\theta_x^*, \theta_y^*$ ) are reconstructed in a given arm by inverting the proton transport equations [26]

$$\theta_x^* = \frac{1}{\frac{dL_x}{ds}} \left( \theta_x - \frac{dv_x}{ds} x^* \right), \quad \theta_y^* = \frac{y}{L_y}, \quad (1)$$

where  $s$  denotes the distance from the interaction point,  $y$  is the vertical coordinate of the proton’s trajectory at the RPs and  $\theta_x = (x_{far} - x_{near})/\Delta s$  is its horizontal angle measured by the RP detectors, whose distance is  $\Delta s = 5.372$  m. The horizontal vertex coordinate  $x^*$  is reconstructed as

$$x^* = \frac{L_{x, far} \cdot x_{near} - L_{x, near} \cdot x_{far}}{d}, \quad (2)$$

where  $d = (v_{x, near} \cdot L_{x, far} - v_{x, far} \cdot L_{x, near})$ . The coefficients  $L_x, L_y$  and  $v_x$  are optical functions of the LHC beam determined by the accelerator magnets. For their definition we refer to [26].

The scattering angles obtained for the two arms are averaged and the four-momentum transfer squared is calculated

$$t = -p^2 \theta^{*2}, \quad (3)$$

where  $p = 1.38$  TeV is the LHC beam momentum and the scattering angle  $\theta^* = \sqrt{\theta_x^{*2} + \theta_y^{*2}}$ . Finally, the azimuthal angle is

$$\phi^* = \arctan \left( \frac{\theta_y^*}{\theta_x^*} \right). \quad (4)$$

#### 3.1.2 RP alignment and beam optics

The alignment is based on the position measurement of the RP movement system, followed by an alignment procedure based on the symmetries of elastic scattering [5, 6]. The residual misalignment with respect to the LHC beam is about  $10 \mu\text{m}$  in the horizontal coordinate and about  $100 \mu\text{m}$  in the vertical. When propagated to the reconstructed scattering angle  $\theta^*$ , this leads to an uncertainty of the order  $5 \mu\text{rad}$ .

The nominal optics has been updated from LHC magnet and current databases and has been calibrated using the observed elastic candidates of DS2, with larger statistics, and validated for DS1 relying on the stability of the LHC optics [21, 25]. The  $\beta^* = 11$  m optics of the LHC is designed with a vertical effective length  $L_y \approx 19.4$  m at the location of the RP detectors; the exact value depends on the location of the detector along the beam. The reconstruction of the horizontal scattering angle uses the derivative of the horizontal effective length  $dL_x/ds \approx -0.4$  at the position of the RPs. The remaining optical functions used in the reconstruction are the horizontal magnifications in the near and far RP, whose value is  $v_{x, near} \approx v_{x, far} \approx -3.2$  and their derivative  $dv_x/ds \approx 4.9 \cdot 10^{-2} \text{ m}^{-1}$ . The different reconstruction formula in the vertical and horizontal plane in Eq. (1) is motivated by their different sensitivity to the LHC magnet and beam perturbations.

The uncertainties of the optical functions are estimated with a Monte Carlo program applying the optics calibration procedure on a sophisticated simulation of the LHC beam and its perturbations [26, 27]. The obtained uncertainty is  $2\%$  for  $dL_x/ds$  and  $3\%$  for  $L_y$ . The uncertainty of the horizontal magnification  $v_x$  and its derivative is  $2\%$  and  $3\%$ , respectively.

#### 3.1.3 Event selection

The analysis follows the similar procedure used for the measurement of the elastic cross section at several other LHC energies: 7 TeV, 8 TeV and 13 TeV [1–9, 21, 28]. The measurement of the elastic rate is based on the selection of events with the following topology in the RP detector system: a reconstructed track in the near and far vertical detectors on one side and a reconstructed track in the near (or far) on the other side of the IP such that the elastic signature is satisfied in one of the two diagonals: left bottom and right top (Diagonal 1) or left top and right bottom (Diagonal 2).

There are four vertical RP detectors along a diagonal, each with slightly different acceptance limitations depending on their vertical distance from the LHC beam. The mentioned topology selection uses only three RPs in order to optimize the statistics of the analysis. In the arm with only one RP the horizontal scattering angle is reconstructed using

$$\theta_x^* = \frac{1}{L_x} (x - v_x \cdot x^*), \quad (5)$$

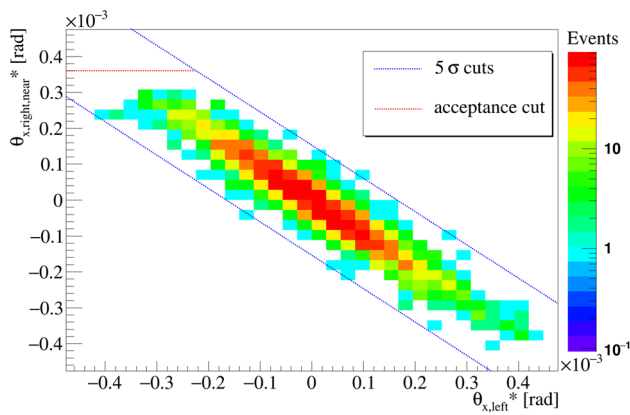


**Fig. 2** The collinearity cut of the two protons using the horizontal scattering angle  $\theta_x^*$ . The red and blue lines show the acceptance and  $5\sigma$  physics cuts, respectively

**Table 1** The physics analysis cuts and their width  $\sigma$  in Diagonal 1 (the other diagonal is in agreement within the quoted uncertainty). The width  $\sigma$  of the horizontal and vertical collinearity cuts define the resolution in the scattering angle, see Fig. 2

Cut name	$\sigma$
1 Vertical collinearity cut	$21.3 \pm 0.4 \mu\text{rad}$
2 y-spectrometer cut, left arm	$51.1 \pm 0.4 \mu\text{m}$
3 x-spectrometer cut, left arm	$69.3 \pm 1.2 \mu\text{m}$
4 Horizontal collinearity cut	$22.3 \pm 0.5 \mu\text{rad}$

where the horizontal vertex coordinate  $x^*$  is calculated from Eq. (2) using the track of the RPs in the other arm of the diagonal.

Besides the topology cut, the elastic event selection requires the collinearity of the outgoing protons in the two arms, see Fig. 2. The diffractive events are suppressed with so-called spectrometer cuts, which require the correlation between the vertical position in the near RP detector  $y_{\text{near}}$  and the inclination  $\Delta y = y_{\text{far}} - y_{\text{near}}$  (and similarly in the horizontal plane), see Table 1. Figure 3 shows the efficiency of the elastic event selection.

Figure 2 shows the horizontal collinearity cut imposing momentum conservation in the horizontal plane. The cuts are applied at the  $5\sigma$  level, and they are optimized for purity (background contamination in the selected sample less than 0.5 %) and for efficiency (uncertainty of true elastic event selection 0.5 %). Figure 3 shows the progressive selection of elastic events.

### 3.1.4 Geometrical and beam divergence correction, unfolding

The vertical acceptance of elastically scattered protons is limited by the RP silicon detector edge and by the LHC magnet apertures. The geometrical acceptance correction is calcu-

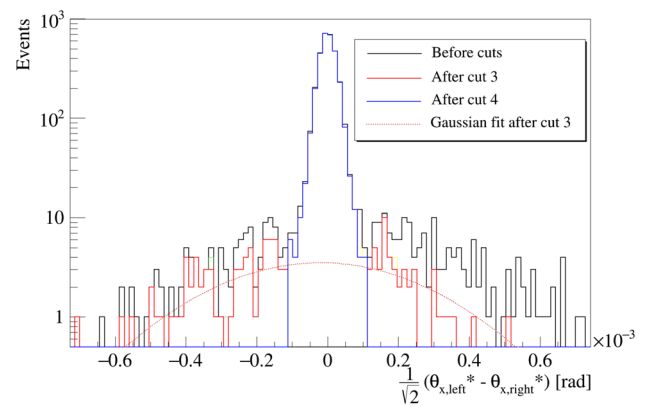


**Fig. 3** The horizontal angular smearing, divergence, of the beam estimated from the data of Diagonal 1. The distribution is shown before any analysis cut (black solid line) and before and after the last cut, see Table 1. The residual background is estimated with a Gaussian fit of the tail before the last analysis cut

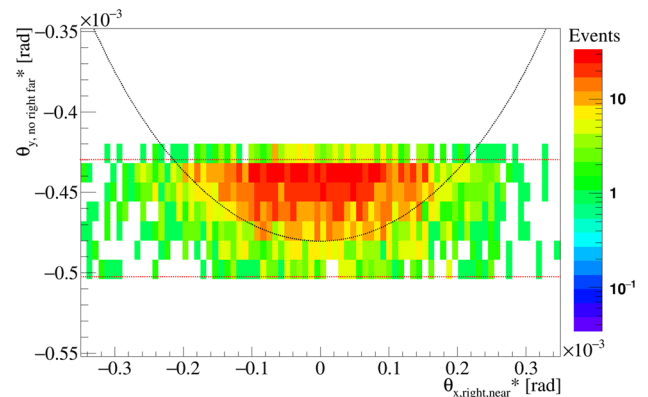


**Fig. 4** Geometrical acceptance cut for Diagonal 1 in the  $(\theta_x^*, \theta_y^*)$  plane. The red lines show the acceptance cuts. In order to optimize the acceptance the right far RP was not used, denoted in  $\theta_{y,\text{no right far}}^*$ , see also Sect. 3.1.3

lated in order to correct for the missing part of the acceptance

$$\mathcal{A}(\theta^*) = \frac{2\pi}{\Delta\phi^*(\theta^*)}, \tag{6}$$

where  $\Delta\phi^*$  is the visible azimuthal angle range, defined by the acceptance cuts, see Fig. 4.

The geometrical acceptance correction formula Eq. (6) assumes the azimuthal symmetry of elastic scattering, which is experimentally verified on the data, see Fig. 5. The acceptance limitations constrain the vertical component  $t_y$  of the analysis to  $|t|_{y,\text{min}} = 0.36 \text{ GeV}^2$  and  $|t|_{y,\text{max}} = 0.48 \text{ GeV}^2$ . The RP distance from the LHC beam is larger than in the earlier TOTEM analyses and the geometrical acceptance correction factor  $\mathcal{A}(t)$  exceeds 5.

The scattering angles are large and reach LHC apertures horizontally. In both diagonals this angular cut has been measured per arm with a dedicated high statistics single arm analysis using 2 RPs. The tighter angular cut for Diagonal 1 is

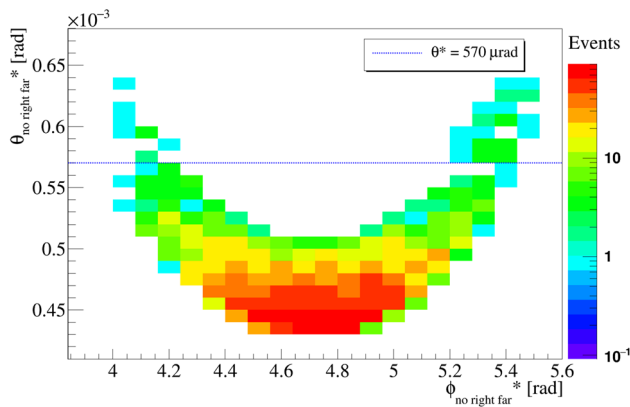


**Fig. 5** The uncorrected distribution of the azimuthal angles  $\phi^*$  per event as a function of  $\theta^*$  in Diagonal 1. The consecutive empty bins along the  $\theta^* = 570 \mu\text{rad}$  line are due to the diffractive minimum at  $t \approx -0.61 \text{ GeV}^2$ , see Fig. 8. In order to optimize the acceptance the right far RP was not used, denoted in  $\phi_{\text{no right far}}^*$ , see also Sect. 3.1.3

in the right arm  $\theta_{x,\text{coll}}^* = +360 \mu\text{rad}$ , which is taken into account in the geometrical acceptance correction  $\mathcal{A}(t)$ , see Fig. 6. The same procedure is applied for Diagonal 2. Figure 6 also provides a reference curve for  $\mathcal{A}(t)$  shown as a blue dashed line without the  $\theta_{x,\text{coll}}^*$  cut.

Close to the acceptance edges there is an additional acceptance loss due to the angular smearing, divergence, of the beam. This additional acceptance loss is modeled with a Gaussian distribution at the corners of the acceptance, with experimentally determined parameters. The model permits to calculate the corresponding vertical beam divergence correction  $\mathcal{D}_v(t_y)$ , see Fig. 6. In the horizontal plane the beam divergence correction  $\mathcal{D}_h(t_x)$  is below 0.5 %.

The unfolding of resolution effects is estimated with a Monte Carlo simulation. The resolution parameters are obtained from the data, see Sect. 3.1.2. The probability distribution  $p(t)$  of the event generator is based on the fit of the differential rate  $dN_{\text{el}}/dt$ . Each generated MC event is propagated to the RP detectors with the proper model of the LHC optics, which takes into account the beam divergence and other resolution effects. The kinematics of the event is reconstructed and a histogram is built from the  $t$  values. The ratio of the histograms without and with resolution effect describes the first approximation of the bin-by-bin corrections due to bin migration. The probability distribution  $p(t)$  of the simulation is multiplied with the correction histogram, to modulate the source, and the procedure is repeated until the histogram with migration effects coincide with the measured distribution, thus the correct source distribution has been found. The uncertainty of the unfolding procedure is estimated from the residual difference between the measured histogram  $dN_{\text{el}}/dt$  and the simulated histogram with resolution effects.

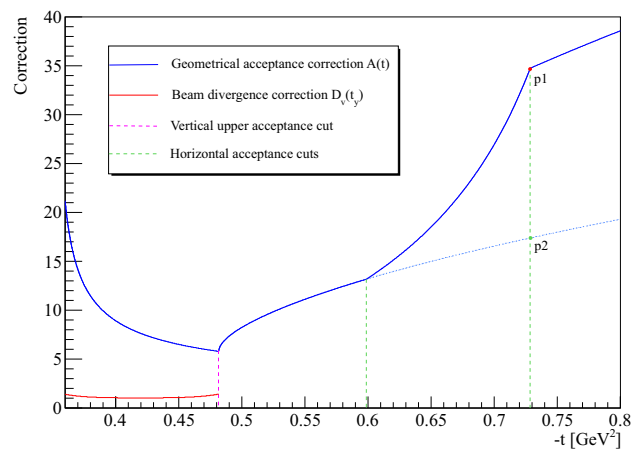


**Fig. 6** The geometrical acceptance correction  $\mathcal{A}(t)$  and the vertical beam divergence correction  $\mathcal{D}_v(t_y)$  for Diagonal 1. The vertical lines indicate the  $|t|$ -positions where the additional acceptance limitations appear due to the vertical and horizontal LHC apertures. The dashed blue line indicates a hypothetical geometrical correction without horizontal acceptance cuts. The ordinate of point  $p1$  is two times the ordinate of  $p2$  at the upper horizontal cut, since the acceptance is halved by the cut at the LHC aperture

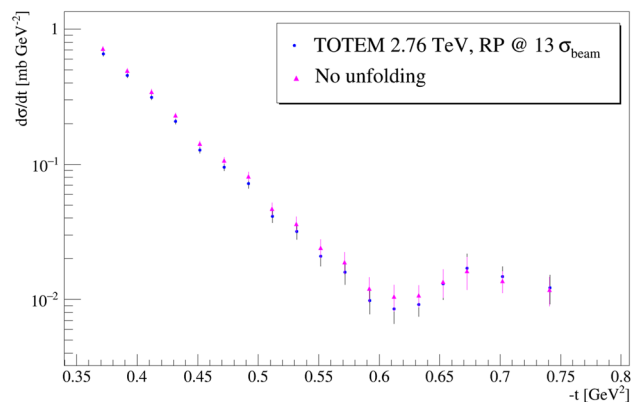


**Fig. 7** The pp differential elastic cross section  $d\sigma/dt$  of DS1 at  $\sqrt{s} = 2.76 \text{ TeV}$  with and without unfolding

The angular spread of the beam is determined with an uncertainty  $0.5 \mu\text{rad}$  by comparing the scattering angles reconstructed from the left and right arm, see Table 1. Therefore the unfolding correction factor  $\mathcal{U}(t)$  can be calculated with a precision better than 0.1 %, see Fig. 7. The event-by-event correction factor due to acceptance corrections and resolution unfolding is

$$\mathcal{C}(t_x, t_y) = \mathcal{A}(t)\mathcal{D}_v(t_y)\mathcal{D}_h(t_x)\mathcal{U}(t). \tag{7}$$

#### 4 The differential cross section

The inefficiency corrections due to pile-up from background and inefficiency due to an additional inefficiency of one RP

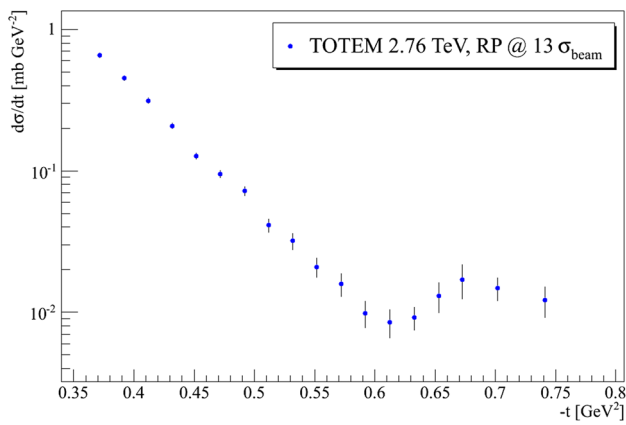


**Fig. 8** The pp differential elastic cross section  $d\sigma/dt$  of DS1 at  $\sqrt{s} = 2.76$  TeV

out of the three used is taken into account with a relative scale factor, computed as a ratio of Diagonal 1 to Diagonal 2 in a representative  $|t|$ -range.

After these corrections the differential rate  $dN_{el}/dt$  of Diagonal 1 and Diagonal 2 agree within their statistical uncertainty over the whole  $|t|$ -range measured. The two diagonals are almost independent measurements, thus the final measured differential rate is calculated as the bin-by-bin weighted average of the two differential elastic rates  $dN_{el}/dt$ , according to their statistical uncertainty.

The overall normalization is determined from the total cross-section analysis at  $\sqrt{s} = 2.76$  TeV, summarized in [7, 21, 28]. The final differential cross-section  $d\sigma/dt$  is obtained by normalizing DS1 to DS2 using the integral of their exponential fits in the overlapping  $t$ -range. The uncertainty on the normalization is about 6 %. The differential cross-section of DS1 is shown in Fig. 8. Figure 9 shows the complete range of the differential cross-section covered by DS1 and DS2. The  $d\sigma/dt$  data points are summarized in Table 2, where the  $|t|$ -dependent systematic uncertainty is also provided. Table 3 contains the data points for DS2.

Figure 9 shows the fit of the diffractive minimum and the possible positions of the subsequent maximum with a third order polynomial in the  $|t|$ -range between 0.47 and 0.74  $\text{GeV}^2$  and beyond. In fact the data determine and characterize the  $t$ -position of the dip  $t_{dip}$ , the cross-section at  $t_{dip}$  and the cross-section at the bump (the local maximum subsequent to the dip) or a lower limit of such cross-section. However, the data do not constrain the  $t$ -position of the bump  $t_{bump}$ , which could be anywhere in the range 0.7 – 0.8  $\text{GeV}^2$  without effecting the corresponding cross-section given the flat derivative (Fig. 9). The dip position is found to be  $|t_{dip}| = (0.61 \pm 0.03) \text{ GeV}^2$ . The overall uncertainty in  $|t|$  (correlated bin-to-bin) is derived from the beam divergence (5 %), alignment (less than 2 %) and unfolding (less than 0.5 %).

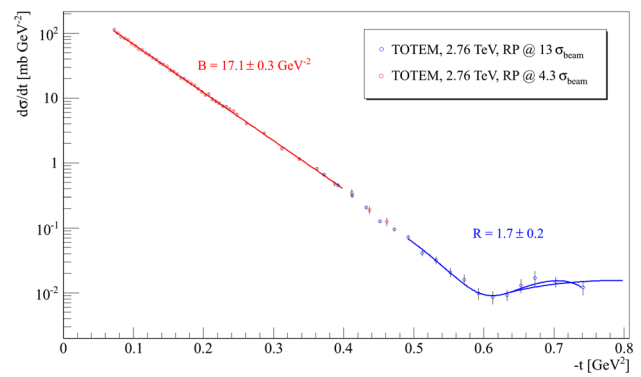


**Fig. 9** The differential cross section  $d\sigma_{el}/dt$  at  $\sqrt{s} = 2.76$  TeV. The figure shows the dataset DS1 (blue hollow circles) and the dataset DS2 of the total cross-section measurement (red hollow circles) used for normalization [7, 21, 28]. The nuclear slope  $B = (17.1 \pm 0.3) \text{ GeV}^{-2}$  and the corresponding fit in the  $|t|$ -range between 0.09  $\text{GeV}^2$  and 0.4  $\text{GeV}^2$  is shown. The fit of the diffractive minimum and maximum with a third order polynomial, for two possible functional forms, is presented in the  $|t|$ -range between 0.47 and 0.74  $\text{GeV}^2$  and beyond

**Table 2** The differential cross-section  $d\sigma/dt$  of DS1 at 2.76 TeV, measured at  $13 \sigma_{beam}$  distance

$ t _{low}$	$ t _{high}$ [ $\text{GeV}^2$ ]	$ t _{repr.}$	$d\sigma/dt$	Statistical uncertainty [ $\text{mb GeV}^{-2}$ ]	Systematic uncertainty
0.3625	0.3825	0.37190	0.6565	0.0277	0.0331
0.3825	0.4025	0.39188	0.4536	0.0183	0.0238
0.4025	0.4225	0.41185	0.3133	0.0140	0.0168
0.4225	0.4425	0.43184	0.2075	0.0091	0.0116
0.4425	0.4625	0.45185	0.1270	0.0062	0.0073
0.4625	0.4825	0.47188	0.0952	0.0056	0.0056
0.4825	0.5025	0.49189	0.0718	0.0054	0.0042
0.5025	0.5225	0.51186	0.0413	0.0044	0.0024
0.5225	0.5425	0.53181	0.0319	0.0041	0.0020
0.5425	0.5625	0.55180	0.0209	0.0033	0.0013
0.5625	0.5825	0.57190	0.0159	0.0029	0.0009
0.5825	0.6025	0.59213	0.0098	0.0021	0.0004
0.6025	0.6225	0.61239	0.0085	0.0019	0.0004
0.6225	0.6425	0.63295	0.0092	0.0017	0.0004
0.6425	0.6625	0.65298	0.0131	0.0031	0.0008
0.6625	0.6825	0.67266	0.0171	0.0047	0.0008
0.6825	0.7225	0.70214	0.0148	0.0027	0.0008
0.7225	0.7625	0.74119	0.0122	0.0030	0.0008

The nuclear slope  $B = (17.1 \pm 0.3) \text{ GeV}^{-2}$  and the corresponding exponential fit in the  $|t|$ -range between 0.09  $\text{GeV}^2$  and 0.4  $\text{GeV}^2$  of the differential cross-section are perfectly consistent with [7, 21, 28].

The differential cross-section  $d\sigma/dt$  is compared to the  $p\bar{p}$  measurement by the D0 experiment [10] in Fig. 10. The measured nuclear slopes before the dip  $B_{pp} = (19.4 \pm$

**Table 3** The differential cross-section  $d\sigma/dt$  of DS2 at  $\sqrt{s} = 2.76$  TeV, measured at  $4.3 \sigma_{\text{beam}}$  distance

$ t _{\text{low}}$	$ t _{\text{high}}$ [GeV <sup>2</sup> ]	$ t _{\text{repr.}}$	$d\sigma/dt$	Statistical uncertainty [mb GeV <sup>-2</sup> ]	Systematic uncertainty
0.0700	0.0750	0.07246	113.88	2.960	1.455
0.0750	0.0800	0.07746	101.14	2.181	1.319
0.0800	0.0850	0.08246	88.78	1.752	1.181
0.0850	0.0900	0.08746	83.25	1.600	1.130
0.0900	0.0950	0.09246	79.25	1.542	1.097
0.0950	0.1000	0.09746	69.81	1.326	0.986
0.1000	0.1050	0.10246	64.27	1.260	0.926
0.1050	0.1100	0.10746	56.75	1.133	0.833
0.1100	0.1150	0.11246	54.96	1.085	0.822
0.1150	0.1200	0.11746	49.43	1.002	0.754
0.1200	0.1250	0.12246	46.41	1.135	0.721
0.1250	0.1300	0.12746	41.59	0.904	0.658
0.1300	0.1350	0.13246	39.28	0.853	0.633
0.1350	0.1400	0.13746	34.87	0.782	0.572
0.1400	0.1450	0.14246	33.42	0.775	0.558
0.1450	0.1500	0.14746	30.92	0.746	0.526
0.1500	0.1550	0.15246	26.78	0.666	0.463
0.1550	0.1600	0.15746	25.73	0.645	0.453
0.1600	0.1650	0.16246	23.32	0.602	0.417
0.1650	0.1700	0.16746	20.63	0.573	0.376
0.1700	0.1750	0.17246	19.84	0.564	0.367
0.1750	0.1800	0.17746	18.14	0.520	0.341
0.1800	0.1850	0.18246	16.68	0.493	0.319
0.1850	0.1900	0.18746	15.61	0.490	0.303
0.1900	0.1950	0.19246	13.99	0.459	0.276
0.1950	0.2000	0.19746	12.55	0.426	0.251
0.2000	0.2050	0.20246	11.21	0.423	0.228
0.2050	0.2100	0.20746	11.56	0.542	0.239
0.2100	0.2150	0.21246	9.59	0.368	0.201
0.2150	0.2200	0.21746	8.95	0.358	0.190
0.2200	0.2250	0.22246	8.34	0.340	0.180
0.2250	0.2300	0.22746	7.47	0.307	0.164
0.2300	0.2350	0.23246	7.35	0.322	0.163
0.2350	0.2400	0.23746	6.72	0.307	0.151
0.2400	0.2450	0.24246	6.28	0.291	0.143
0.2450	0.2500	0.24746	5.58	0.269	0.129
0.2500	0.2750	0.26161	4.08	0.103	0.098
0.2750	0.3000	0.28661	2.87	0.089	0.074
0.3000	0.3250	0.31161	1.66	0.064	0.045
0.3250	0.3500	0.33661	1.15	0.056	0.033
0.3500	0.3750	0.36161	0.82	0.044	0.025
0.3750	0.4000	0.38661	0.47	0.036	0.015
0.4000	0.4250	0.41161	0.34	0.045	0.012
0.4250	0.4500	0.43661	0.19	0.024	0.007
0.4500	0.4750	0.46161	0.13	0.018	0.005

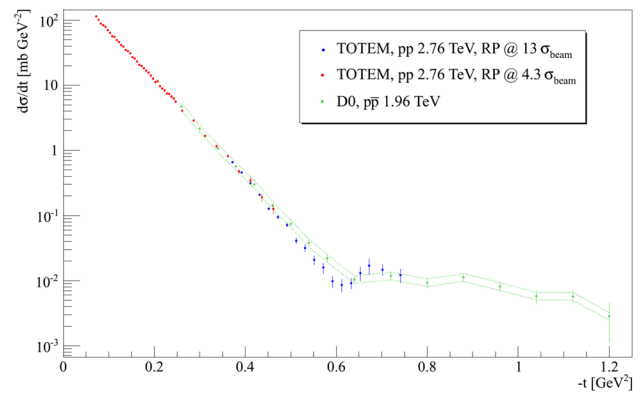


**Fig. 10** The differential cross sections  $d\sigma/dt$  at  $\sqrt{s} = 2.76$  TeV measured by the TOTEM experiment and the elastic  $p\bar{p}$  measurement of the D0 experiment at 1.96 TeV [10]. The green dashed line indicates the normalization uncertainty of the D0 measurement

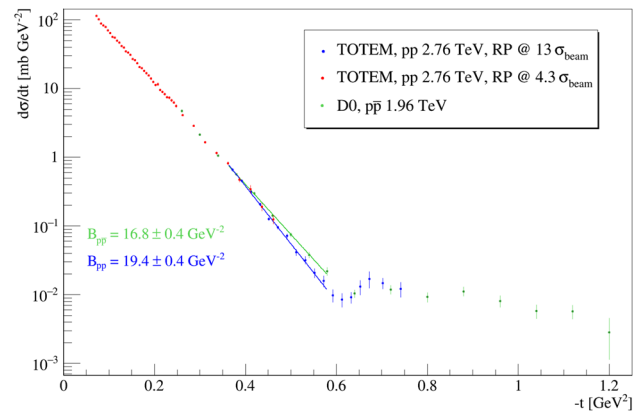


**Fig. 11** The exponential fit of the differential cross sections  $d\sigma/dt$  at  $\sqrt{s} = 2.76$  TeV measured by the TOTEM experiment and the elastic  $p\bar{p}$  measurement of the D0 experiment at 1.96 TeV in the  $|t|$ -range from 0.36 to 0.58 GeV<sup>2</sup>. The pp differential cross section shows a steepening before the dip, and the slope parameters in this range quantify another key parameter to claim the significant deviation of pp and  $p\bar{p}$

0.4) GeV<sup>-2</sup> and  $B_{p\bar{p}} = (16.8 \pm 0.4) \text{ GeV}^{-2}$  are key parameters to quantify the difference between pp and  $p\bar{p}$ , see Fig. 11. According to the nuclear slope difference, the significance of the incompatibility between the pp vs.  $p\bar{p}$  is greater than  $4\sigma$ . Recently, Refs. [29,30], pointed out that the  $t$ -dependent nuclear slope parameter  $B(t) = \frac{d}{dt} \ln(d\sigma/dt)$  indicates a clear Odderon effect as  $B_{pp}(t) \neq B_{p\bar{p}}(t)$ .

A dedicated Monte Carlo simulation has been used to simulate all analysis steps in order to model the correct propagation of the central values and their uncertainties. The simulation resulted in uncertainty corrections mainly due to the asymmetry of Poisson distributions in the bins which have lower statistics. The uncertainty on the  $d\sigma/dt$  ratio at the bump to that at the dip,  $R$ , has been determined with similar MC studies.

## 5 Discussion of the results

The TOTEM experiment at CERN LHC has observed the presence of a diffractive minimum at  $\sqrt{s} = 2.76$  TeV in elastic pp scattering with high significance. The importance of this observation is that the new data measured at  $\sqrt{s} = 2.76$  TeV are rather close in energy to the D0 results of p $\bar{p}$  measured at  $\sqrt{s} = 1.96$  TeV.

The measured ratio of the pp differential cross-section at the bump and dip is  $R = 1.7 \pm 0.2$ , see Fig. 9. The pp data also shows a steepening of the differential cross-section and a change in the nuclear slope  $B(t)$  starting at  $|t| \approx 0.4$  GeV<sup>2</sup> (Fig. 11). Both features are absent in the p $\bar{p}$  data measured at  $\sqrt{s} = 1.96$  TeV of the D0 experiment, where a kink structure without a minimum and a subsequent maximum can be observed with  $R_{p\bar{p}} = 1.0 \pm 0.1$ . This value  $R_{p\bar{p}}$  and its uncertainty can be obtained by fitting the published D0 data in the  $t$ -range of the plateau (nearly constant  $d\sigma/dt$ ), including and after the kink [10]. Therefore, the incompatibility on the  $R$  parameter between the p $\bar{p}$  data at  $\sqrt{s} = 1.96$  TeV and the pp data at 2.76 TeV is approximately  $3\sigma$ .

At higher LHC energies of 7 TeV and 13 TeV, the dip has been observed already earlier by TOTEM [1, 9]. It is evidently a persistent structure in pp elastic scattering at LHC energies.

As far as we know, there are no models which are able to describe the pp TOTEM data and the p $\bar{p}$  D0 data (total cross-section,  $\rho$ , dip-region) without the effects of the Odderon [31–33]. On the contrary, theoretical models including the effects of the Odderon have predicted the observed effects and are able to describe both the pp TOTEM data and the p $\bar{p}$  D0 data (TeV scale) [11, 34].

Therefore, unless the 800 GeV energy difference provokes considerable effects, the significant difference between the pp and p $\bar{p}$  differential cross-section provides evidence for the exchange of a colourless C-odd three-gluon compound state in the  $t$ -channel of the proton–proton elastic scattering.

The observed difference between pp and p $\bar{p}$  is the most classic definition of evidence for the Odderon since the last day of run at the ISR (more than 40 years ago) [35–37]. While at lower energies the diffractive dip contributions may naturally come from secondary Reggeons, their contribution is generally considered negligible, less than 1 %, at LHC energies due to their Regge trajectory intercept lower than unity [20].

A variety of odd-signature exchanges relevant at high energies have been discussed in literature, within different frameworks and under different names, see e.g. the review [19]. The “Odderon” was introduced within the axiomatic theory as an amplitude contribution responsible for the difference between pp and p $\bar{p}$  differential cross-section in the dip region. Crossing-odd trajectories were also studied within the framework of Regge theory as a counterpart of the crossing-even Pomeron. It has also been shown that such an

object must exist in QCD, as a colourless compound state of three gluons with quantum numbers  $J^{PC} = 1^{--}$  (see e.g. [13–17], for reviews see [18, 19]). The binding strength among the 3 gluons is greater than the strength of their interaction with other particles. There is also evidence for a three-gluon compound state in QCD lattice calculations, known under the name “vector glueball” (see e.g. [38]). A three-gluon compound state, on one hand, can be exchanged in the  $t$ -channel and contribute, e.g., to the elastic scattering amplitude. On the other hand it can be created in the  $s$ -channel and thus be observed in spectroscopic studies, as it is suggested by the  $s$ - $t$  channel duality [39].

There are multiple ways how an odd-signature exchange component may manifest itself in observable data. Focussing on elastic scattering at the LHC (unpolarised beams), there are 3 regions often argued to be sensitive. In general, the effects of an odd-signature exchange (compound state of 3 gluons in leading order) are expected to be much smaller than those of even-signature exchanges (compound state of 2 gluons in leading order). Consequently, the sensitive regions are those where the contributions from two-gluon compound state exchanges cancel or are small. At very low- $|t|$  the two-gluon amplitude is expected to be almost purely imaginary, while a three-gluon exchange would make contributions to the real part and therefore  $\rho$ , the ratio of the real to imaginary part of the nuclear scattering amplitude, is a very sensitive parameter. The  $\sigma_{\text{tot}}$  and  $\rho$  parameter measurement of the TOTEM experiment at  $\sqrt{s} = 13$  TeV already provided the first indication for the existence of a colourless C-odd three-gluon compound state [7, 8, 32, 34].

Sometimes the high- $|t|$  region is also argued to be sensitive to three-gluon exchanges since the contribution from 2-gluon exchanges is rapidly decreasing. However, large- $|t|$  TOTEM data at 13 TeV [9] indicate that this region is either dominated by a perturbative-QCD amplitude, see e.g. [40] or approximately follows a constituent quark behaviour [41, 42].

The third opportunity is the comparison of the dip range, exploited in this analysis. The dip is often described as the  $t$ -range where the imaginary part of the amplitude is crossing zero, thus ceding the dominance to the real part to which a three-gluon exchange may contribute. In agreement with such predictions, the observed dips in p $\bar{p}$  scattering are shallower than those in pp. There are data at  $\sqrt{s} = 53$  GeV showing a significant difference between the pp and p $\bar{p}$  dip [37]. The interpretation of this difference is, however, complicated due to a possible non-negligible contribution from secondary Reggeons. These are not expected to give sizeable effects at the Tevatron energies, which thus gives weight to the interpretation of the D0 observation of a very shallow dip in p $\bar{p}$  elastic scattering [10] compared to the very pronounced dip measured by TOTEM at 2.76 TeV (this paper), 7 TeV [1] and 13 TeV [9].

## 6 Summary

The proton–proton elastic differential cross section  $d\sigma/dt$  has been measured by the TOTEM experiment at  $\sqrt{s} = 2.76$  TeV LHC energy with  $\beta^* = 11$  m beam optics. The differential cross-section can be described with an exponential in the range  $0.36 < |t| < 0.54$  GeV<sup>2</sup>, followed by a significant diffractive minimum at  $|t_{\text{dip}}| = (0.61 \pm 0.03)$  GeV<sup>2</sup>. The ratio of the  $d\sigma/dt$  between the bump (the local maximum subsequent to the dip) and dip is  $R = 1.7 \pm 0.2$ . This value  $R$  is significantly different from  $R_{p\bar{p}} = 1.0 \pm 0.1$ , obtained from the  $p\bar{p}$  measurement of the D0 experiment at  $\sqrt{s} = 1.96$  TeV.

In case the 800 GeV energy difference (between this TOTEM measurement and the D0 measurement [10]) is not responsible for the observed difference between them, as indicated by the broad energy range of pp and  $p\bar{p}$  measurements from 500 GeV to 13 TeV, the results provide evidence for a colourless C-odd 3-gluon compound state exchange in the  $t$ -channel of the proton–proton and proton–antiproton elastic scattering. The presented observables  $R$  and the nuclear slope before the dip  $B_{pp}$  ( $B_{p\bar{p}}$ ) are both  $\sqrt{s}$  dependent, and this dependence has to be studied in detail in order to quantify the exact significance of the observation. This will be the subject of a forthcoming joint publication by the TOTEM and D0 experiments.

**Acknowledgements** We are grateful to the beam optics development team for providing the beams and operating the instrumentation, to the machine coordinators and the LPC coordinators for scheduling the dedicated fills. This work was supported by the institutions listed on the front page and partially also by NSF (US), the Magnus Ehrnrooth Foundation (Finland), the Waldemar von Frenckell Foundation (Finland), the Academy of Finland, the Finnish Academy of Science and Letters (The Vilho Yrjö and Kalle Väisälä Fund), the Circles of Knowledge Club (Hungary) and the OTKA NK 101438 and the EFOP-3.6.1-16-2016-00001 grants (Hungary). Individuals have received support from Nylands nation vid Helsingfors universitet (Finland), MSMT CR (the Czech Republic), the János Bolyai Research Scholarship of the Hungarian Academy of Sciences, the NKP-17-4 New National Excellence Program of the Hungarian Ministry of Human Capacities and the Polish Ministry of Science and Higher Education Grant no. MNiSW DIR/WK/2017/07-01.

**Data Availability Statement** This manuscript has no associated data or the data will not be deposited. [Authors' comment: The datasets analysed in this manuscript are available from the corresponding author on a reasonable request.]

**Open Access** This article is licensed under a Creative Commons Attribution 4.0 International License, which permits use, sharing, adaptation, distribution and reproduction in any medium or format, as long as you give appropriate credit to the original author(s) and the source, provide a link to the Creative Commons licence, and indicate if changes were made. The images or other third party material in this article are included in the article's Creative Commons licence, unless indicated otherwise in a credit line to the material. If material is not included in the article's Creative Commons licence and your intended use is not permitted by statutory regulation or exceeds the permit-

ted use, you will need to obtain permission directly from the copyright holder. To view a copy of this licence, visit <http://creativecommons.org/licenses/by/4.0/>.  
Funded by SCOAP<sup>3</sup>.

## References

1. G. Antchev, et al. Proton–proton elastic scattering at the LHC energy of  $\sqrt{s} = 7$  TeV. (TOTEM collaboration). EPL **95**(4), 41001 (2011). <https://doi.org/10.1209/0295-5075/95/41001>
2. G. Antchev, et al. First measurement of the total proton–proton cross section at the LHC energy of  $\sqrt{s} = 7$  TeV. (TOTEM collaboration). EPL **96**, 21002 (2011). <https://doi.org/10.1209/0295-5075/96/21002>
3. G. Antchev et al., Measurement of proton–proton elastic scattering and total cross-section at  $\sqrt{s} = 7$  TeV. EPL **101**(2), 21002 (2013a). <https://doi.org/10.1209/0295-5075/101/21002>
4. G. Antchev, et al. Luminosity-independent measurement of the proton–proton total cross section at  $\sqrt{s} = 8$  TeV. (TOTEM collaboration). Phys. Rev. Lett. **111**(1), 012001 (2013). <https://doi.org/10.1103/PhysRevLett.111.012001>
5. G. Antchev et al., Evidence for non-exponential elastic proton–proton differential cross-section at low  $|t|$  and  $\sqrt{s}=8$  TeV by TOTEM. (TOTEM collaboration). Nucl. Phys. B **899**, 527–546 (2015). <https://doi.org/10.1016/j.nuclphysb.2015.08.010>
6. G. Antchev, et al. Measurement of elastic pp scattering at  $\sqrt{s} = 8$  TeV in the Coulomb-nuclear interference region: determination of the  $\rho$ -parameter and the total cross-section. (TOTEM collaboration). Eur. Phys. J. C **76**(12), 661 (2016). <https://doi.org/10.1140/epjc/s10052-016-4399-8>
7. G. Antchev, et al. First measurement of elastic, inelastic and total cross-section at  $\sqrt{s} = 13$  TeV by TOTEM and overview of cross-section data at LHC energies. (TOTEM collaboration). Eur. Phys. J. C **79**(2), 103 (2019). <https://doi.org/10.1140/epjc/s10052-019-6567-0>. arXiv:1712.06153
8. G. Antchev et al., First determination of the  $\rho$  parameter at  $\sqrt{s} = 13$  TeV: probing the existence of a colourless C-odd three-gluon compound state. Eur. Phys. J. C **79**(9), 785 (2019b). <https://doi.org/10.1140/epjc/s10052-019-7223-4>. arXiv:1812.04732
9. G. Antchev et al., Elastic differential cross-section measurement at  $\sqrt{s} = 13$  TeV by TOTEM. Eur. Phys. J. C **79**(10), 861 (2019c). <https://doi.org/10.1140/epjc/s10052-019-7346-7>. arXiv:1812.08283
10. V.M. Abazov et al. Measurement of the differential cross section  $d\sigma/dt$  in elastic  $p\bar{p}$  scattering at  $\sqrt{s} = 1.96$  TeV. (D0 collaboration). Phys. Rev. D **86**, 012009 (2012). <https://doi.org/10.1103/PhysRevD.86.012009>
11. L. Lukaszuk, B. Nicolescu, A possible interpretation of pp rising total cross-sections. Lett. Nuovo Cim **8**, 405–413 (1973). <https://doi.org/10.1007/BF02824484>
12. D. Joynson, E. Leader, B. Nicolescu, C. Lopez, NonRegge and HyperRegge effects in pion-nucleon charge exchange scattering at high-energies. Nuovo Cim A **30**, 345 (1975). <https://doi.org/10.1007/BF02730293>
13. J. Kwiecinski, M. Praszalowicz, Three gluon integral equation and odd C singlet regge singularities in QCD. Phys. Lett. B **94**, 413–416 (1980). [https://doi.org/10.1016/0370-2693\(80\)90909-0](https://doi.org/10.1016/0370-2693(80)90909-0)
14. J. Bartels, High-energy behavior in a nonabelian gauge theory (II). Nucl. Phys. B **175**, 365–401 (1980). [https://doi.org/10.1016/0550-3213\(80\)90019-X](https://doi.org/10.1016/0550-3213(80)90019-X)
15. T. Jaroszewicz, J. Kwiecinski, Odd C gluonic regge singularities of perturbative QCD and their decoupling from deep inelastic neutrino scattering. Z. Phys. C **12**, 167 (1982). <https://doi.org/10.1007/BF01548613>

16. R.A. Janik, J. Wosiek, Solution of the odderon problem. *Phys. Rev. Lett.* **82**, 1092–1095 (1999). <https://doi.org/10.1103/PhysRevLett.82.1092>
17. J. Bartels, L.N. Lipatov, G.P. Vacca, A New odderon solution in perturbative QCD. *Phys. Lett. B* **477**, 178–186 (2000). [https://doi.org/10.1016/S0370-2693\(00\)00221-5](https://doi.org/10.1016/S0370-2693(00)00221-5). [arXiv:hep-ph/9912423](https://arxiv.org/abs/hep-ph/9912423)
18. M.A. Braun., Odderon and QCD (1998). [arXiv:hep-ph/9805394](https://arxiv.org/abs/hep-ph/9805394)
19. C. Ewerz, The Odderon in quantum chromodynamics. (2003). [arXiv:hep-ph/0306137](https://arxiv.org/abs/hep-ph/0306137)
20. L. Jenkovszky, I. Szanyi, C.I. Tan, Shape of proton and the pion cloud. *Eur. Phys. J. A* **54**(7), 116 (2018). <https://doi.org/10.1140/epja/i2018-12567-5>. [arXiv:1710.10594](https://arxiv.org/abs/1710.10594)
21. F.J. Nemes, Elastic and total cross-section measurements by TOTEM: past and future. *PoS DIS* **2017**, 059 (2018). <https://doi.org/10.22323/1.297.0059>
22. G. Anelli, et al. The TOTEM experiment at the CERN Large Hadron Collider. (TOTEM collaboration). *JINST* **3**, S08007 (2008). <https://doi.org/10.1088/1748-0221/3/08/S08007>
23. G. Antchev, et al. (TOTEM collaboration), TOTEM Upgrade Proposal. (2013). <https://cds.cern.ch/record/1554299>
24. G. Ruggiero et al., Characteristics of edgeless silicon detectors for the Roman Pots of the TOTEM experiment at the LHC. *Nucl. Instrum. Methods A* **604**, 242–245 (2009). <https://doi.org/10.1016/j.nima.2009.01.056>
25. O.S. Bruning, P. Collier, P. Lebrun, S. Myers, R. Ostojic, J. Poole, P. Proudlock, LHC Design Report (Monographs, CERN, Geneva, CERN Yellow Reports, 2004). <https://doi.org/10.5170/CERN-2004-003-V-1>. <https://cds.cern.ch/record/782076>
26. G. Antchev, et al. LHC optics measurement with proton tracks detected by the roman pots of the TOTEM experiment. (TOTEM collaboration). *New J. Phys.* **16**, 103041 (2014). <https://doi.org/10.1088/1367-2630/16/10/103041>
27. F. Nemes. Elastic scattering of protons at the TOTEM experiment at the LHC. Ph.D. thesis, Eötvös U., CERN-THESIS-2015-293 (2015)
28. G. Antchev, et al. Measurement of proton–proton elastic scattering and total cross-section at  $\sqrt{s} = 2.76$  TeV. (TOTEM collaboration) (2020) (**in preparation**)
29. E. Martynov, B. Nicolescu, Odderon effects in the differential cross-sections at Tevatron and LHC energies. *Eur. Phys. J. C* **79**(6), 461 (2019). <https://doi.org/10.1140/epjc/s10052-019-6954-6>. [arXiv:1808.08580](https://arxiv.org/abs/1808.08580)
30. T. Csörgő, R. Pasechnik, A. Ster, Odderon and proton substructure from a model-independent Levy imaging of elastic  $pp$  and  $p\bar{p}$  collisions. *Eur. Phys. J. C* **79**(1), 62 (2019). <https://doi.org/10.1140/epjc/s10052-019-6588-8>. [arXiv:1807.02897](https://arxiv.org/abs/1807.02897)
31. J.R. Cudell, V.V. Ezhela, P. Gauron, K. Kang, YuV Kuyanov, S.B. Lugovsky, E. Martynov, B. Nicolescu, E.A. Razuvaev, N.P. Tkachenko, Benchmarks for the forward observables at RHIC, the Tevatron Run II and the LHC. *Phys. Rev. Lett.* **89**, 201801 (2002). <https://doi.org/10.1103/PhysRevLett.89.201801>
32. V.A. Khoze, A.D. Martin, M.G. Ryskin, Elastic proton–proton scattering at 13 TeV. *Phys. Rev. D* **97**(3), 034019 (2018). <https://doi.org/10.1103/PhysRevD.97.034019>. [arXiv:1712.00325](https://arxiv.org/abs/1712.00325)
33. V.A. Khoze, A.D. Martin, M.G. Ryskin, High energy elastic and diffractive cross sections. *Eur. Phys. J. C* **74**(2), 2756 (2014). <https://doi.org/10.1140/epjc/s10052-014-2756-z>. [arXiv:1312.3851](https://arxiv.org/abs/1312.3851)
34. E. Martynov, B. Nicolescu, Did TOTEM experiment discover the Odderon? *Phys. Lett. B* **778**, 414–418 (2018). <https://doi.org/10.1016/j.physletb.2018.01.054>. [arXiv:1711.03288](https://arxiv.org/abs/1711.03288)
35. A. Breakstone et al., A measurement of  $\bar{p}p$  and  $pp$  elastic scattering in the dip region at  $\sqrt{s} = 53$ -GeV. *Phys. Rev. Lett.* **54**, 2180 (1985). <https://doi.org/10.1103/PhysRevLett.54.2180>
36. A. Breakstone et al., A measurement of  $\bar{p}p$  and  $pp$  elastic scattering at ISR energies. *Nucl. Phys. B* **248**, 253–260 (1984). [https://doi.org/10.1016/0550-3213\(84\)90595-9](https://doi.org/10.1016/0550-3213(84)90595-9)
37. U. Amaldi, K.R. Schubert, Impact parameter interpretation of proton proton scattering from a critical review of All ISR data. *Nucl. Phys. B* **166**, 301–320 (1980). [https://doi.org/10.1016/0550-3213\(80\)90229-1](https://doi.org/10.1016/0550-3213(80)90229-1)
38. C.J. Morningstar, M.J. Peardon, The Glueball spectrum from an anisotropic lattice study. *Phys. Rev. D* **60**, 034509 (1999). <https://doi.org/10.1103/PhysRevD.60.034509>. [arXiv:hep-lat/9901004](https://arxiv.org/abs/hep-lat/9901004)
39. G. Veneziano, Construction of a crossing-symmetric, Regge behaved amplitude for linearly rising trajectories. *Nuovo Cim A* **57**, 190–197 (1968). <https://doi.org/10.1007/BF02824451>
40. A. Donnachie, P.V. Landshoff, Elastic scattering at large  $t$ . *Z. Phys. C* **2**, 55 (1979). (**Erratum: Z. Phys. C2,372(1979)**)
41. V.A. Matveev, R.M. Muradian, A.N. Tavkhelidze, Automodelism in the large-angle elastic scattering and structure of hadrons. *Lett Nuovo Cim* **7**, 719–723 (1973). <https://doi.org/10.1007/BF02728133>
42. S.J. Brodsky, G.R. Farrar, Scaling laws at large transverse momentum. *Phys. Rev. Lett.* **31**, 1153–1156 (1973). <https://doi.org/10.1103/PhysRevLett.31.1153>